EVALUATING THE ACCURACY OF CONVENTIONAL DRAG PREDICTION AND VALIDATION METHODS FOR SMALL ELECTRIC UAVS

Leonid Heide

University of Minnesota: Twin Cities

July 28, 2019

Abstract

The cost-effectiveness and versatility of unmanned aerial vehicles (UAVs) has led to an increase in demand for small, fixed-wing, electric aircraft. Aircraft performance characteristics such as flight time, efficiency, and turn performance rely on the amount of air resistance that the vehicle experiences. The force caused by air resistance is known as the drag force, and accurate drag predictions are essential to aircraft design, control, and mission planning. This study seeks to evaluate the accuracy of calculating the drag of small electric UAVs using a common empirical method for fixed-wing aircraft, and to determine the efficacy of using glide tests to validate drag values. Glide tests are performed to measure drag of three aircraft, and wind-tunnel testing conducted to measure the drag generated by windmilling propellers. The component drag build-up method is then implemented to analytically determine drag, and the results compared to the data. It is demonstrated that by accounting for the unique operating conditions of small UAVs, the component drag build-up method can be used to accurately determine drag. It is also shown that glide tests are an effective method to experimentally determine drag and validate predicted values.

1. Introduction

Due to their low cost and simplicity, the use of small electric unmanned aerial vehicles (UAVs) has proliferated in recent years [7]. As the demand for UAVs grows, methods to accurately model and validate flight characteristics are needed. Critical to aircraft design and flight performance analysis is the determination of the vehicle's air resistance (aerodynamic drag) [2].

Many tools are readily available for accurate drag analysis of conventional aircraft. A common and simple method used to predict drag is the component drag build-up method (CDBM), where the total drag is the aggregate of the drag contributions of the individual aircraft components [14]. Empirical techniques to determine these components, such as those described by Raymer [14], Roskam [15], and Hoerner [8], are reliable standards in the aeronautical community derived from extensive analysis of conventional fixed-wing aircraft that operate at high Reynolds numbers (around $1.5*10^6$) [10]. The Reynolds number is an important scaling factor in aerodynamics, and represents the ratio of inertial to viscous forces experienced by a body as it moves through a fluid [2]. However, unlike conventional aircraft, the small size of electric UAVs coupled with their lower operational velocities results in significantly smaller Reynolds numbers (between $6*10^4$ and $4*10^5$) [17]. At these Reynolds numbers boundary layer conditions are unsteady due to turbulent flows and laminar separation bubbles [10], thereby resulting in higher skin friction drag [1]. Furthermore, elements such as physical protrusions, blunt surfaces, and propulsion systems tend to be large

relative to overall size of small UAVs and contribute a significant amount of drag. Such unique attributes of small UAVs makes drag analysis using conventional empirical methods directly unreliable.

Analytical methods of drag prediction such as those employed in modern high-fidelity computational fluid dynamics (CFD) have increased in their accuracy due to rapid progress of computing power. Despite these advancements, CFD-based drag predictions for small UAVs are currently challenging due to the difficulties of modeling turbulence, viscous flows, and flows over bluff bodies [4]. In addition, performing CFD simulations is expensive, time-consuming, and requires access to high-speed supercomputers, which makes these methods impracticable to most groups.

Validation of drag predictions is important for the improvement of drag models. Wind-tunnel testing, CFD simulations, and flight-testing are commonly employed to measure drag of conventional aircraft and optimize predictive methods. Wind-tunnel testing is an effective means to test drag, but is limited by the availability of suitable facilities. Furthermore, wind-tunnel data which would be useful for small UAV drag analysis is not as plentiful as the material available for conventional aircraft. Flight testing is another effective way to determine drag, and various flight test methods to determine fixed wing aircraft characteristics are described in work such as that of Ralph Kimberlin [9]. One simple method to determine the drag of an aircraft is to perform a series of unpowered glides at various velocities [9,12]. The low cost and risk associated with UAVs makes flight testing significantly more feasible when compared to conventional aircraft.

This study demonstrates that drag can be predicted using a modified component drag build up method, and validated using unpowered glide tests. Three aircraft belonging to the University of Minnesota Uninhabited Aerial Vehicle lab were equipped with an airspeed sensor, GPS, and flight controller. The aircraft were subjected to a series of glide tests, and the data used to evaluate drag over a range of velocities. Due to uncertainty regarding the drag contribution of a windmilling propeller, wind-tunnel tests were performed on two propeller-motor configurations. The drag data was then used to modify the component drag build up method and demonstrate that the predicted curves fall within the error bounds of the measured drag. It was concluded that the drag generated by a small electric UAV can be evaluated using a modified component drag build up method, and that glide testing is an effective means to measure drag.

2. Component Drag Build Up

2.1 General Equations

The drag force (D) exerted on an aircraft is determined by the equation [11]:

(2.1.1) $D = \frac{1}{2}\rho U^2 S_{ref} C_D$

Where (ρ) is density of the free-stream, (U) is the velocity of the free-stream, and (S_{ref}) is the aircraft's reference area. Total drag consists of a lift-dependent (induced) component (C_{di}) and a lift-independent (parasitic) component (C_{dp}) [11]:

(2.1.2) $C_D = C_{dp} + C_{di}$

The coefficient of induced drag (C_{di}) was calculated using the equation [11]:

(2.1.3) $C_{di} = Q_i \frac{C_L^2}{\pi ARe}$

Where (AR) is the wing's aspect-ratio, (e) is the span efficiency factor, and (C_L) is the coefficient of lift. A multiplier (Q_i) was applied as a corrective factor to account for trim force, as the control surfaces on small electric UAVs are large relative to the reference area. The coefficient of lift was calculated assuming that steady level flight conditions were satisfied [11]:

(2.1.4) $C_L = \frac{2W}{\rho U^2 S_{ref}}$

Where (W) is the aircraft's weight in Newtons. The coefficient of parasitic drag (C_{dp}) was calculated using the equation [14]:

(2.1.5) $C_{dp} = Q_p \left[\frac{\Sigma(C_f FF_c S_{wet_c})}{S_{ref}} + C_{dp}{}_{propeller} + C_{dp}{}_{landing\ gear} + C_{dp}{}_{flat\ plate} \right]$

Where C_f is the skin friction coefficient, FF_c is the form factor of the component, and S_{wet_c} is the wetted area of the component. Drag contributions due to interference and unaccounted factors are represented by a multiplier (Q_p). Drag contributed by the propeller$(C_{dp}{}_{propeller})$, and landing gear $(C_{dp}{}_{landing\ gear})$ are also added. Since conventional component drag build-up methods assume a streamlined body, and one of the aircraft tested had a rectangular fuselage with a bluff nose, drag caused by a flat plate of an area equal to the fuselage's cross sectional area (A_{max}) was added$(C_{dp}{}_{flat\ plate})$ [2]:

(2.1.6) $C_{dp}{}_{flat\ plate} = \frac{1.2 A_{max}}{S_{ref}}$

To account for a wind-milling propeller $(C_{d}{}_{propeller})$, wind-tunnel drag data was used. The data was also compared to a propeller drag prediction method described by Raymer [14]:

(2.1.7) $C_{d0}{}_{propeller} = \frac{0.8 \sigma A_{propeller\ disk}}{S_{ref}}$

(2.1.8) $\sigma = \frac{n_{blade}}{AR_{blade} \pi}$

Where (n_{blade}) is the number of blades, $(A_{propeller\ disk})$ is the frontal area of the propeller disk, and (AR_{blade}) is the blade aspect ratio. Additionally, the landing gear was accounted for:

(2.1.9) $C_{d0}{}_{landing\ gear} = \frac{0.25 A_{tire} + 0.05 A_{strut}}{S_{ref}}$

Where (A_{tire}) and (A_{strut}) are the frontal cross-sectional areas of the tire and strut respectively.

2.2 Skin Friction Coefficient Equations

To evaluate and compare the effect of different boundary layer models on the drag of the aircraft, the skin friction coefficient (C_f) was determined using three models. The first method $\left(C_{f_{Hybrid}}\right)$from "*Boundary Layer Theory*" by Hermann Schlichting assumes a "hybrid" boundary layer, where the laminar flow transitions into a turbulent flow [16]:

(2.2.1) $C_{f_{Hybrid}} = \frac{0.455}{(log_{10}R_L)^{2.58}} - \frac{A}{R_L}$

Where the Reynolds number (R_L) is based on the wing chord length [2], The constant (A) was determined using the lower critical Reynold's number for the aircraft's airfoil and a table provided in "*Boundary Layer Theory*"[16,6].

The second method ($C_{f_{Laminar}}$) assumes a fully laminar boundary layer, and is determined using Blasius's equation for incompressible flow [17,13]:

(2.2.2) $C_{f_{Laminar}} = \frac{1.32824}{\sqrt{log_{10}R_L}}$

The third method ($C_{f_{Turbulent}}$) assumes a fully turbulent boundary layer, and is determined using Schlichting's equation for incompressible, turbulent flow [16]:

(2.2.3) $C_{f_{Turbulent}} = \frac{0.455}{(log_{10}R_L)^{2.58}}$

2.3 Form Factor Equations

To determine the form factors(FF) of the aircraft components, four different equation sets were compared and evaluated. The first set of equations (FF_{Raymer}) are presented by Raymer [14]. The form factors of the wing, horizontal stabilizer, and vertical stabilizer were evaluated using the equation [14]:

(2.3.1) $FF_{Raymer_{wing\ \&\ stabilizers}} = \left[1 + \frac{0.6}{\left(\frac{x}{c}\right)_m}\left(\frac{t}{c}\right) + 100\left(\frac{t}{c}\right)^4\right] * [1.34M^{0.18}]$

Where $\left(\frac{x}{c}\right)_m$ is the chord-wise location of maximum thickness, $\left(\frac{t}{c}\right)$ is the airfoil thickness to chord ratio, and (M) is the Mach number. The fuselage's form factor was calculated using [14]:

(2.3.2) $FF_{Raymer_{fuselage}} = 1 + \frac{60}{f^3} + \frac{f}{400}$

(2.3.3) $f = \frac{l}{\sqrt{\left(\frac{4}{\pi}\right)A_{max}}}$

Where (l) is the maximum thickness, and (A_{max}) is the maximum frontal area (assuming a smooth surface).

The second set of equations, ($FF_{Hoerner}$) described by Hoerner [8,13]:

(2.3.4) $FF_{Hoerner_{wing\ \&\ stabilizers}} = 1 + 2\left(\frac{t}{c}\right) + 60\left(\frac{t}{c}\right)^4$

(2.3.5) $FF_{Hoerner_{fuselage}} = 1 + \frac{1.5}{(\frac{l}{d})^{1.5}} + \frac{7}{(\frac{l}{d})^3}$

Where (d) is the fuselage diameter (Hoerner assumes a streamlined body). Since the fuselages of the aircraft tested were not circular, their diameter was estimated by taking the distance from the cross sectional centroid to the outermost wall.

The third set of equations, (FF_{Covert}) described by Covert [3,13]:

(2.3.6) $$FF_{Covert\ wing\ \&\ stabilizers} = 1 + 1.8\left(\frac{t}{c}\right) + 50\left(\frac{t}{c}\right)^4$$

(2.3.7) $$FF_{Covert\ fuselage} = 1.02\left(1 + \frac{1.5}{\left(\frac{l}{d}\right)^{1.5}} + \frac{7}{(1-M^3)^{0.6}\left(\frac{l}{d}\right)^3}\right)$$

The fourth form-factor (FF_{EDET}) equation was developed by Feagin [5,13] to describe wings with conventional airfoils. There is no unique form factor equation for the fuselage, so Hoerner's equation was used:

(2.3.8) $$FF_{EDET\ wing\ \&\ stabilizers} = 1 + \frac{t}{c}\left(2.94 + \frac{t}{c}\left(7.17 + \frac{t}{c}\left(48.89 + \frac{t}{c}\left(-1403.02 + \frac{t}{c}\left(8598.76 + \frac{t}{c}(-15834.3)\right)\right)\right)\right)\right)$$

3. Ground Testing

Wind tunnel experiments were performed in order to determine whether the equations (2.1.7) and (2.1.8) accurately predicted drag generated by a windmilling propeller.

3.1 Methodology

In order to accurately determine the drag contributed by windmilling propellers during flight testing, tests were conducted in combination with aircraft motors. To replicate glide conditions, the breaks on the motors were activated. Using the wind tunnel in Akerman Hall at the University of Minnesota, the drag of a 12x6" CAM folding propeller and a 12x6" thin electric APC propeller was measured at several airspeeds within the flight envelopes of the test aircraft. Tests were performed with only the motor and spinner, and then with the entire propeller-spinner-motor assembly. This allowed for both the drag contributed by the propeller and the motor-spinner combination to be determined.

3.2 Results

Figures 3.2.1 and 3.2.2 display the data obtained from the propeller wind tunnel tests. The breaking prevented the propeller from rotating until after the airspeed reached 9.3 m/s. Due to the active coils in the electric motors, the propellers did not start completing full, uninterrupted rotations until after 12 m/s. Furthermore, the drag remained effectively zero until after 9.3 m/s.

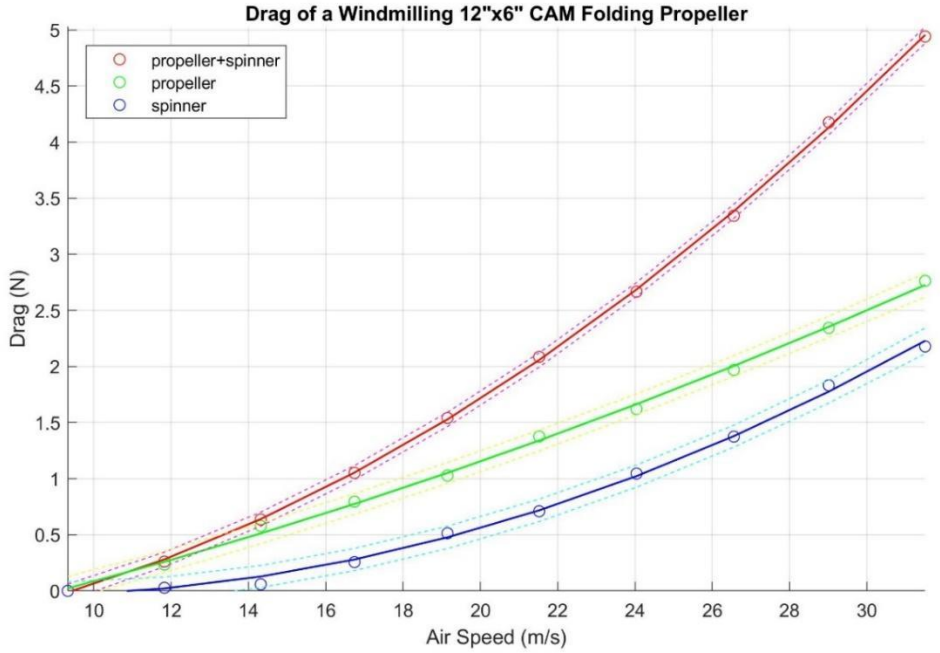

Figure 3.2.1: Wind tunnel data obtained from a windmilling 12”x6” CAM folding propeller, with 95% prediction intervals (Note, the propeller did not fold during wind tunnel or glide testing).

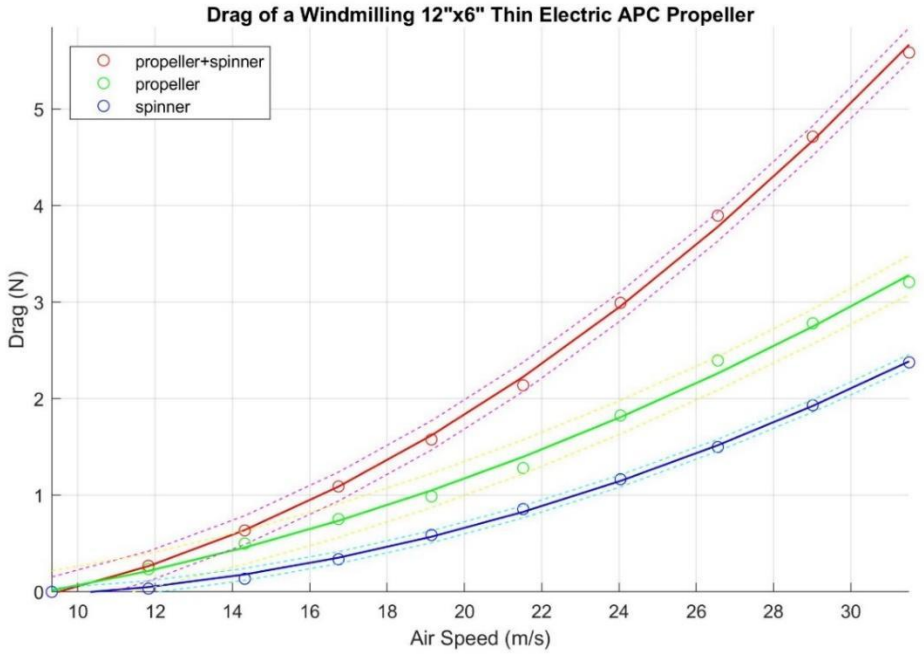

Figure 3.2.2: Wind tunnel data obtained from a windmilling 12”x6” thin electric APC propeller, with 95% prediction intervals.

4. Flight Testing

4.1 Methodology

Three small electric UAVs from the University of Minnesota UAV lab were equipped with air data sensors, a GPS, and a flight controller/data collector. A general description of the aircraft is provided in Table 4.1.1:

Table 4.1.1: Test Aircraft Descriptions

Aircraft	Motor Configuration	Nose Description	Wing Span (m)	Wing Aspect Ratio	Reference Area (m^2)	Wetted Area (m^2)	Weight (N)
Ultra-Stick 25e "Thor"	Single electric tractor motor mounted on fuselage nose	Flat Plate (Bluff)	1.26	5.11	0.311	1.30	17.8
XUAV Talon "Ullr"	Single electric pusher motor mounted on fuselage aft	Paraboloid (Not Bluff)	2.15	7.35	0.627	1.91	24.4
Strix Stratosurfer	Single electric pusher motor mounted on top of the fuselage	Filleted complex geometry (Not Bluff)	1.58	8.49	0.293	0.99	12.8

Table 4.1.1: General descriptions and parameters of test aircraft.

The aircraft were subjected to a series of controlled glides during which the airspeed was adjusted through elevator deflection. It is essential to hold the velocity constant in order to satisfy steady flight conditions. The aircraft altitude and airspeed was recorded throughout the flights, and the experiment repeated twice for each vehicle.

4.2 Obtaining Drag from Data

The altitude and airspeed of the aircraft was interpolated and then filtered, in order to remove data noise and average the phugoid motion. The velocity was then integrated to determine the aircraft displacement during the glide. The data was graphed (as shown in Figure A.1) and manually inspected to identify intervals for which steady level flight conditions were satisfied. A satisfactory test interval is shown in Figure A.2, characterized by a constant descent rate and velocity. Conversely, a noisy test interval which does not satisfy steady flight conditions is shown in Figure A.3.

The glide angle (γ) can be expressed in through the equation:

(4.2.1) $\gamma = \left[\frac{\Delta h}{\Delta d}\right]$

Where (Δd) is the displacement obtained through the integration of velocity, and (Δh) is the altitude displacement. The glide angle can then be used to obtain the equation for Drag [11]:

(4.2.2) $D = W \, sin \, sin \, \gamma$

Which can be simplified:

(4.2.3) $D = W \frac{\Delta h}{\Delta d}$

Equation 4.2.3 was used to obtain drag over the drag over the input sampling intervals.

4.3 Results

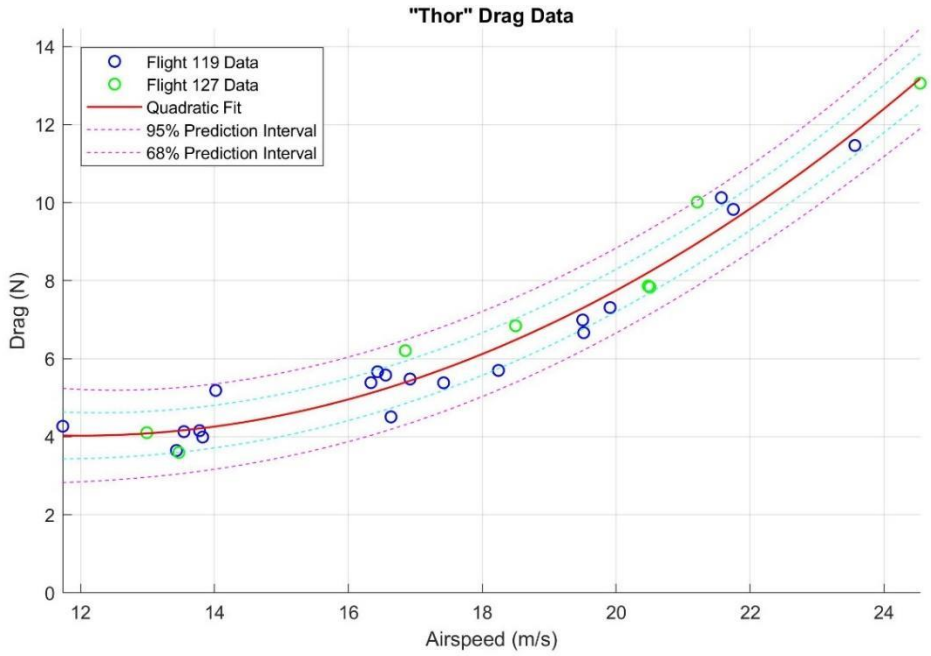

Figure 4.3.1: Drag Data obtained from two “Thor” flights.

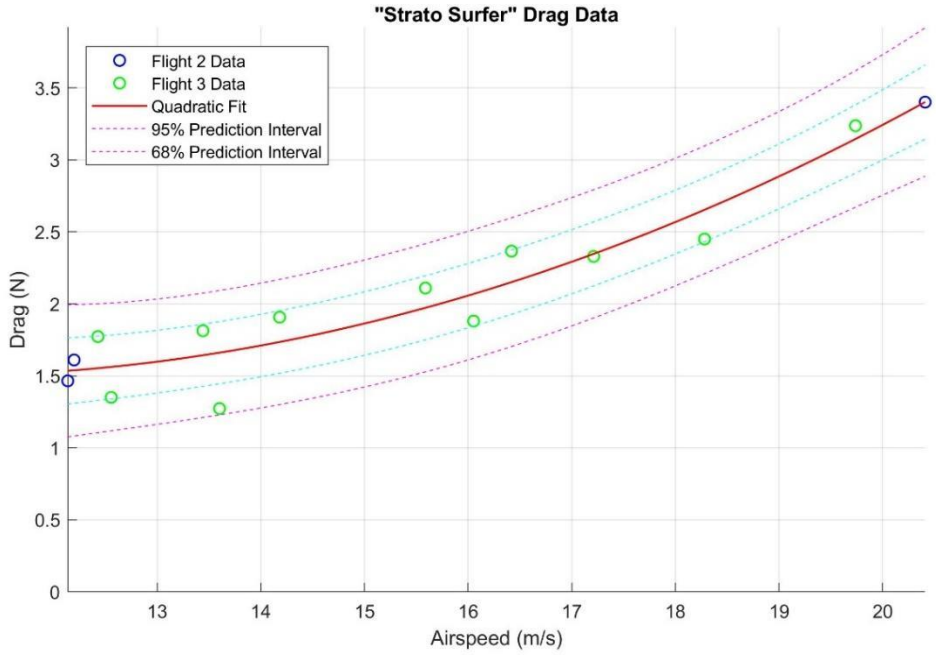

Figure 4.3.2: Drag Data obtained from two “Strato Surfer” flights.

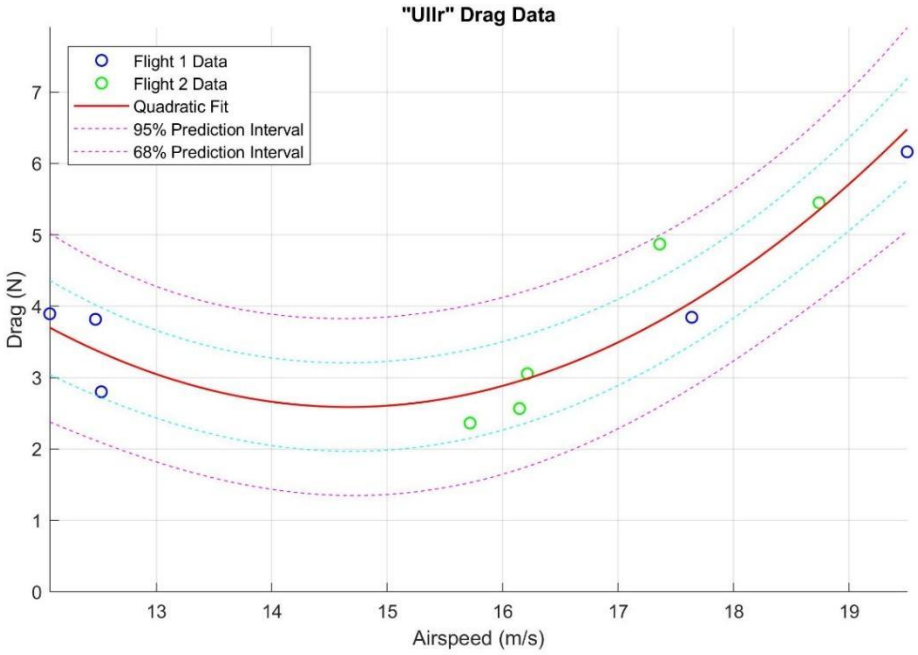

Figure 4.3.3: Drag Data obtained from two "Ullr" flights.

5. Discussion

5. 1 Evaluating Glide Test Data

Drag generated by small UAVs is heavily dominated by parasitic drag, and the minimum drag value (where $C_{dp} = C_{di}$) lies at or below the tested flight envelope [6,12,17]. As parasitic drag is a second order polynomial with no first or zero order variables, the drag data collected can be expected to follow a quadratic trend. The validity of the drag data can therefore be assessed by assigning a quadratic fit to the points. The flight test data for "Thor" (Figure 4.3.1) and "Strato Surfer" (Figure 4.3.1) clearly follow this trend, and it can therefore be concluded that the data for these aircraft is valid. This is also confirmed by the low noise and low phugoid motion observed in the data (Figure A.2).

The "Ullr" drag data (Figure 4.3.3) on the other hand, does not follow this trend, and exhibits greater sparsity. The glide tests for this aircraft were problematic, as there was significant oscillation during the descent caused by the autopilot being unable to hold a constant velocity. The phugoid motion and noise was substantial enough to make it difficult to filter (as seen in Figure A.3). This issue can be rectified in future experiments by adjusting the autopilot or performing the glides manually. It is therefore concluded that the "Ullr" data is unreliable for these glide tests.

5.2 Evaluating Propeller Drag Data and Comparison to Prediction

The propeller drag data exhibited parasitic drag trends as expected, making it possible to fit quadratic curves to the points. It can be concluded that the propeller data is reliable. The folding propeller (used on "Ullr"

and “Thor”) was compared to the propeller drag prediction summarized in equations 2.1.7 and 2.1.8. Figure 5.2.1 shows that past 11.38 m/s the predicted windmilling propeller drag is smaller than the measured drag. It should be noted that Raymer’s propeller prediction does not account for mechanical resistance contributed by the motor. The drag generated by the spinner and motor are also significant. The component drag build up was therefore performed using the wind tunnel propeller data rather than equations 2.1.7 and 2.1.8.

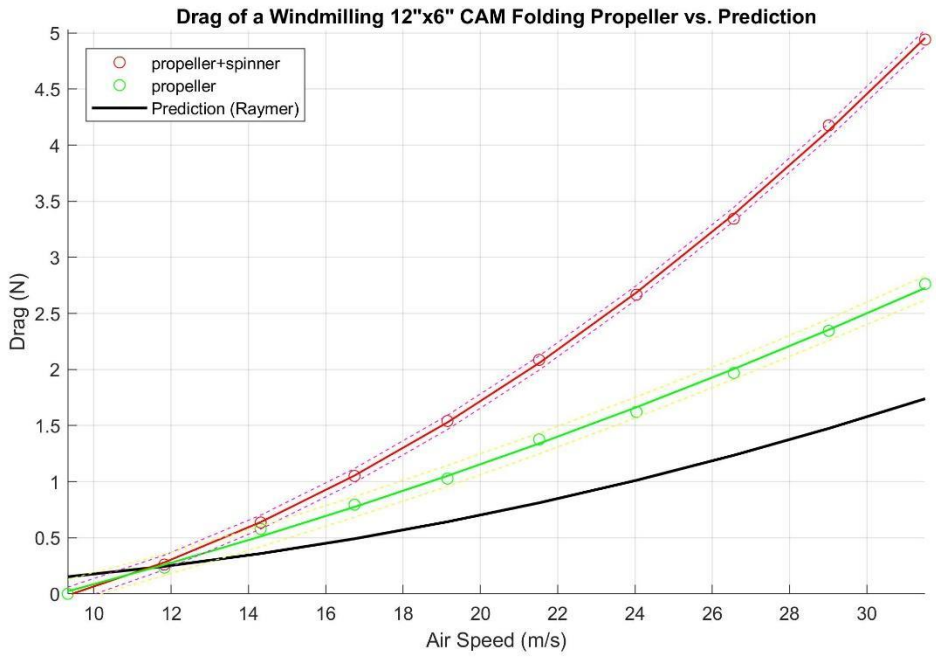

Figure 5.2.1: Experimental vs. predicted propeller drag

5.3 Component Drag Build Up Implementation

In order to determine the experimental parasitic drag, the predicted induced drag was subtracted from the drag data:

(5.3.1) $D_{real\ parasitic} = D_{real\ total} - D_{predicted\ induced}$

The dominance of the parasitic drag for small electric UAVs means that this operation can be performed even with some uncertainty in the induced drag prediction. Although this may cause an offset at lower free stream velocities, the evaluated experimental parasitic drag value will become more accurate towards higher air speeds as induced drag decays.

The experimental parasitic drag was used to validate that the boundary layers on the tested aircraft are fully-turbulent (equation 2.2.3). Parasitic drag was predicted three times using the coefficient of friction equations presented in section 2.2, and compared to the experimental data. This is demonstrated in Figure 5.3.1 using the “Strato Surfer”: the predicted drag using the turbulent model closely matches the experimental drag data. This observation is compatible with theory, as the low chord Reynolds number and physical features such as a large propeller wash, protrusions, and physical imperfections cause turbulence.

In a study performed in 2018 [6] it was proposed that the form factor equations had a significant impact on drag prediction methods. To determine the impact of choosing different form factor equations on the accuracy of the prediction, the parasitic drag was calculated using the equation sets described in section 2.3. The predicted drag was plotted against the experimentally determined parasitic drag, as shown in Figure 5.3.2 in the case of the Strato Surfer. The data closely match the predictions made by the Hoerner (equations 2.3.4 and 2.3.5) form factor equations, which were used for the remainder of this study. Although there are other form factor equations readily available [13], the variation between the form factor models was not as significant as proposed in the 2018 study [6]. In situations where the streamlined body assumption does not hold, as in the case of "Thor", adjustments must be made to account for bluff body drag. To resolve this discrepancy, drag generated by a flat plate equal in area to the fuselage's cross section was added to the predicted parasitic drag (as shown in 2.1.6). This operation was only necessary for "Thor", as "Ullr" and "Strato Surfer" are streamlined. Assumptions made for large aircraft regarding the "cleanliness" of the surfaces, low interference drag, and dynamic pressure uniformity cannot be made for small electric UAVs. Resistance caused by external features such as antennae, GPS modules, and pitot-static probes is negligible on conventional aircraft. However, the large relative size of these components on small electric UAVs results in a significant amount of interference and pressure drag. These effects were accounted for by adjusting the factor (Q_p) in equation 2.1.5. It was observed that the drag prediction for "Thor", which has more drag inducing features, benefitted from higher Q_p values (approx. 1.35) compared to the cleaner and more streamlined "Strato-Surfer" (approx. 1.25). In order to maintain consistency, a Q_p value of 1.30 was used for all three aircraft. The trim drag correction factor (Q_i) described in equation 2.1.3 was also adjusted to improve the induced drag prediction (approx. 1.10 for all aircraft). This can be justified by the large relative size of the control surfaces on small electric UAVs.

Figure 5.3.2 shows a summary of component contributions to total parasitic drag for "Thor". The drag generated by the fuselage is relatively small (since a streamlined body is assumed), however the drag generated by the flat plate is very large. The validity adding a flat plate to the total drag can be evaluated in future tests by comparing the drag generated by an aircraft in a "streamlined" configuration (with a nose cone) with the drag generated by the same aircraft in a "bluff" configuration (with a flat plate nose). The contribution of the windmilling propeller and and interference drag (drag caused by the inclusion of factor Q_p) is significant. Additional data is needed to determine what values of Q best represent the conditions present in small UAVs.

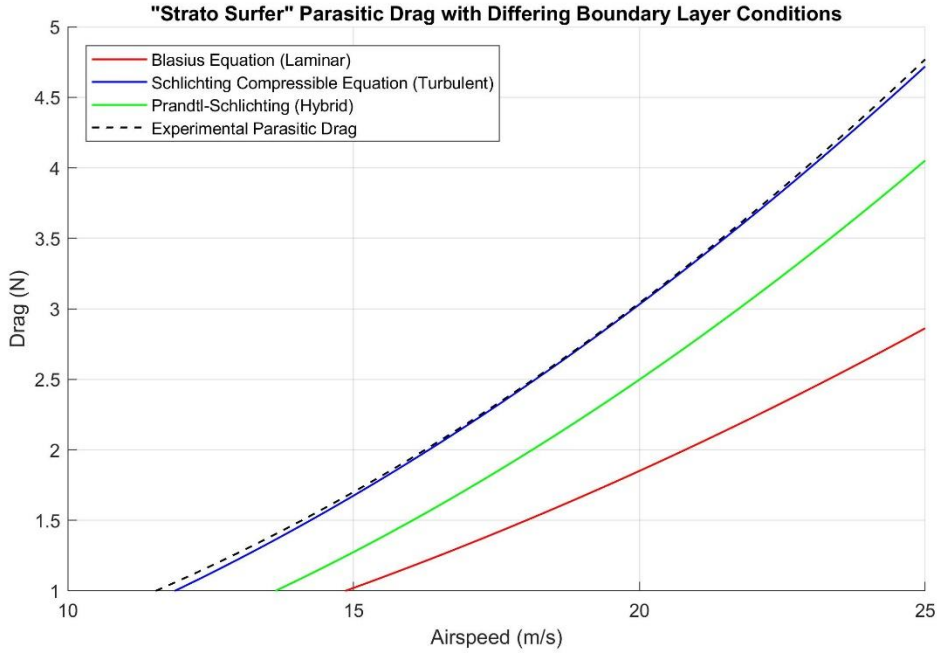

Figure 5.3.1: Parasitic drag predictions for the "Strato Surfer" using three different boundary layer models vs. experimentally determined parasitic drag.

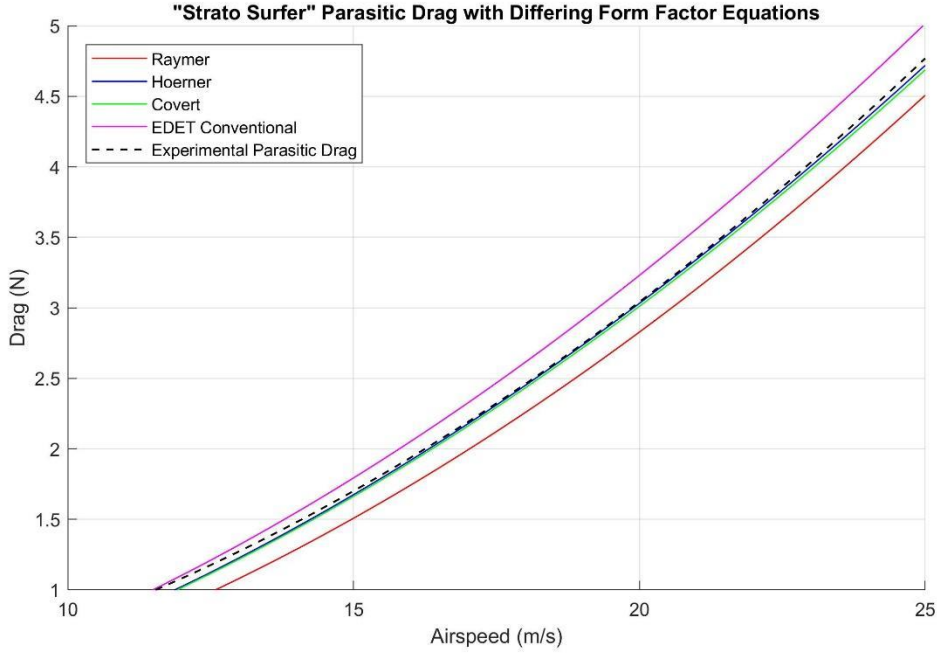

Figure 5.3.2: Parasitic drag predictions for the "Strato Surfer" using four different form factor equations vs. experimentally determined drag.

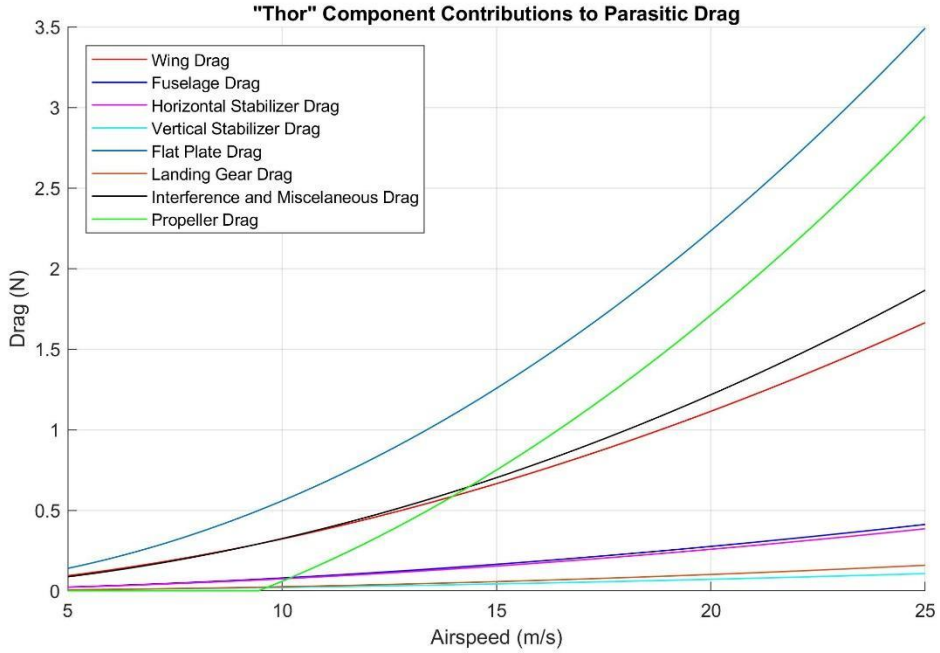

5.4 Comparing Glide Test Data to Predictions

Using the adjustments to the component drag build up method described in section 5.2, drag predictions were made for all three aircraft and compared to the test data. Plots showing predicted drag vs. experimental drag are shown

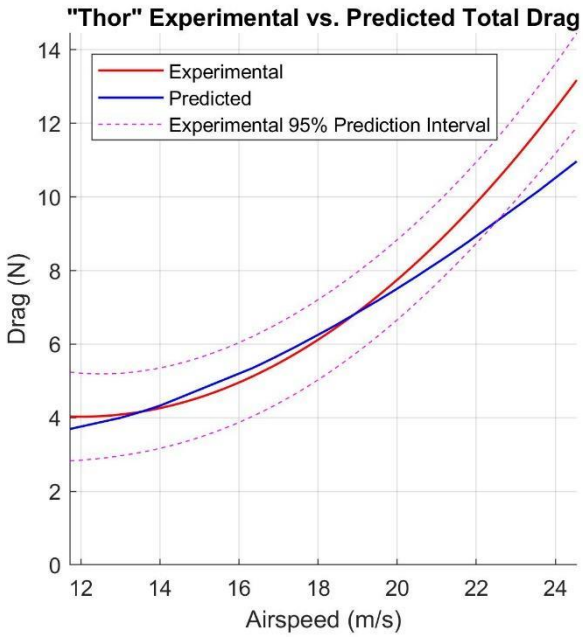

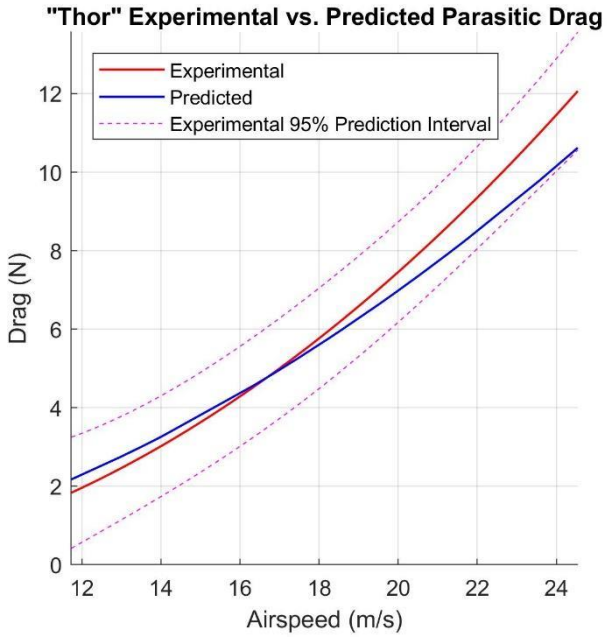

Figures 5.4.1 and 5.4.2: Experimental vs. predicted total and parasitic drag for "Thor"

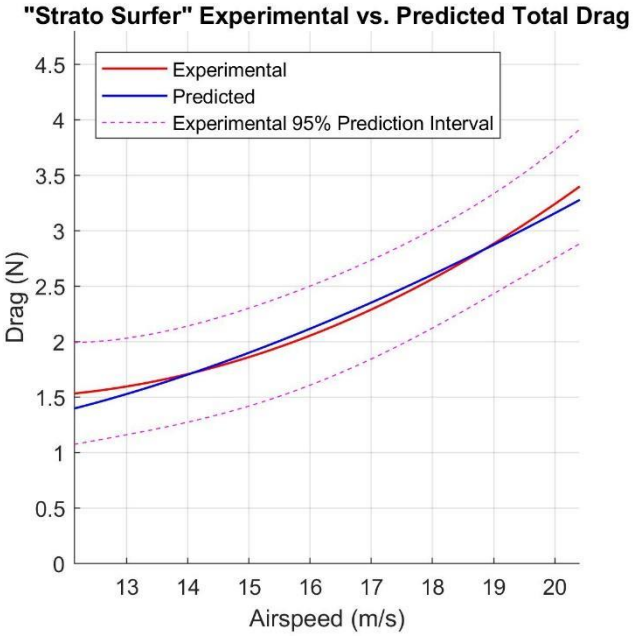

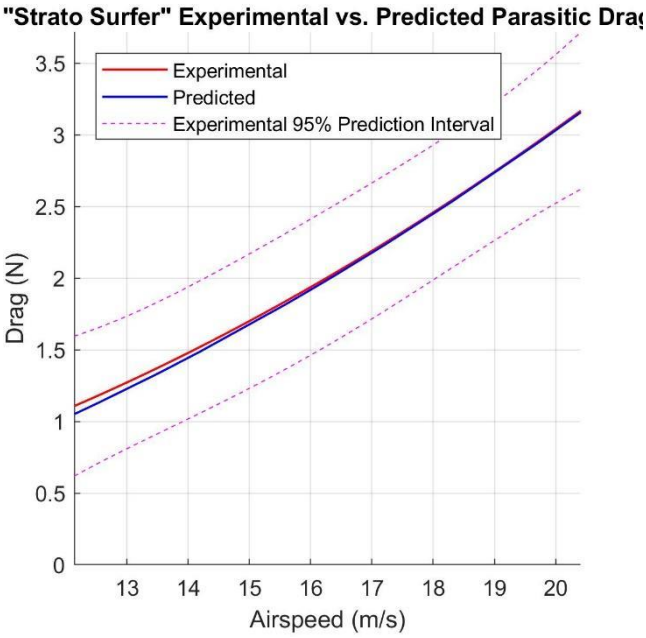

Figures 5.4.3 and 5.4.4: Experimental vs. predicted total and parasitic drag for "Strato Surfer"

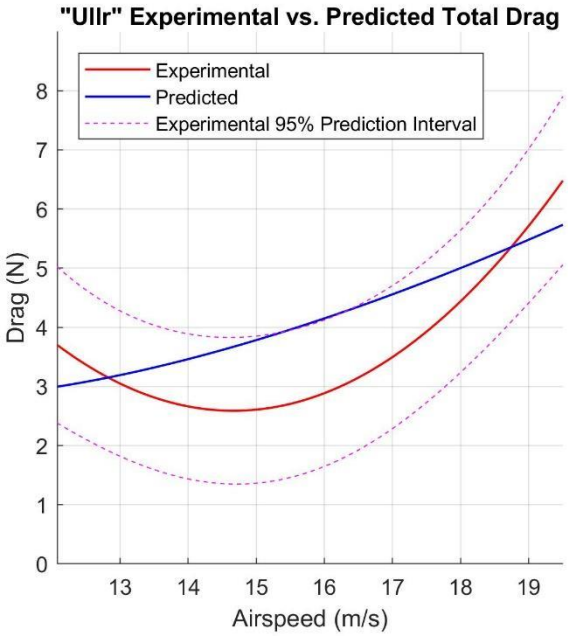

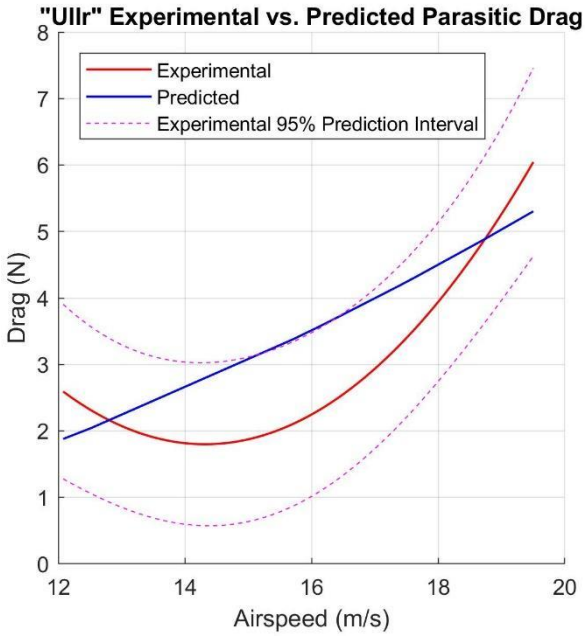

Figures 5.4.5 and 5.4.6: Experimental vs. predicted total and parasitic drag for "Ullr"

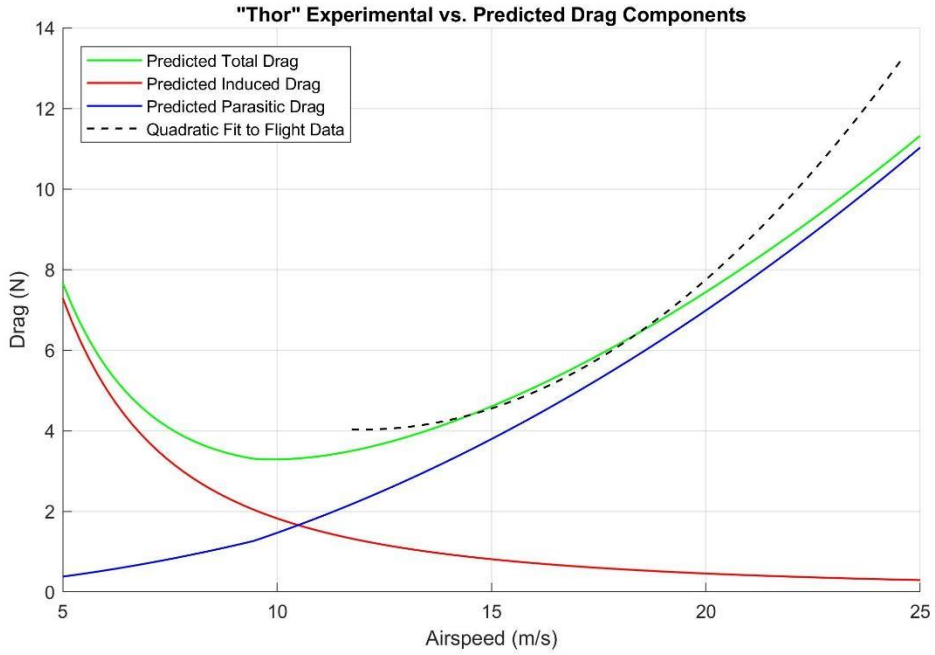

Figure 5.3.7: Experimental vs. predicted drag for "Thor"

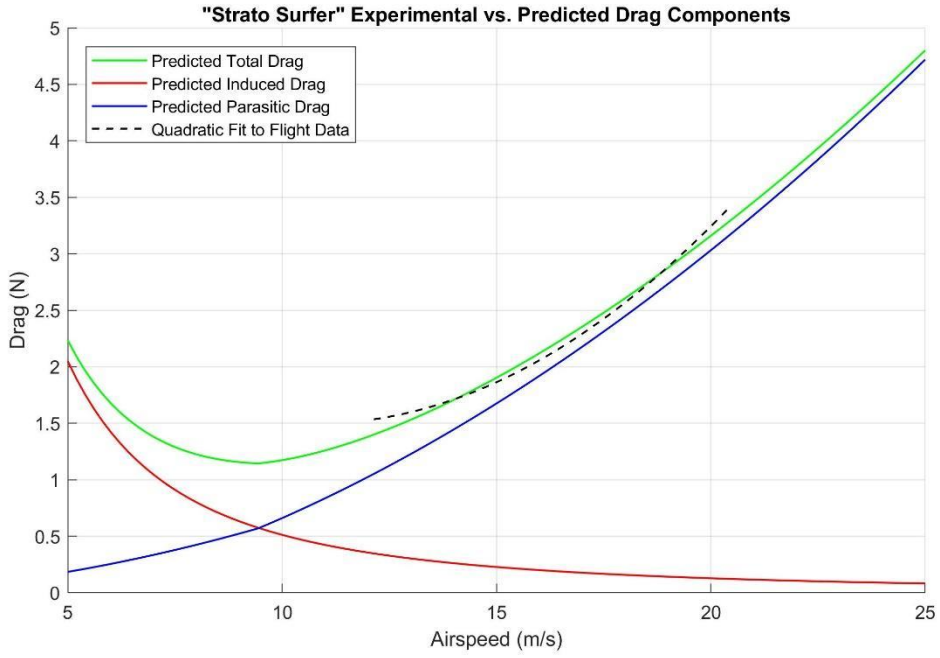

Figure 5.3.8: Experimental vs. predicted drag for "Strato Surfer"

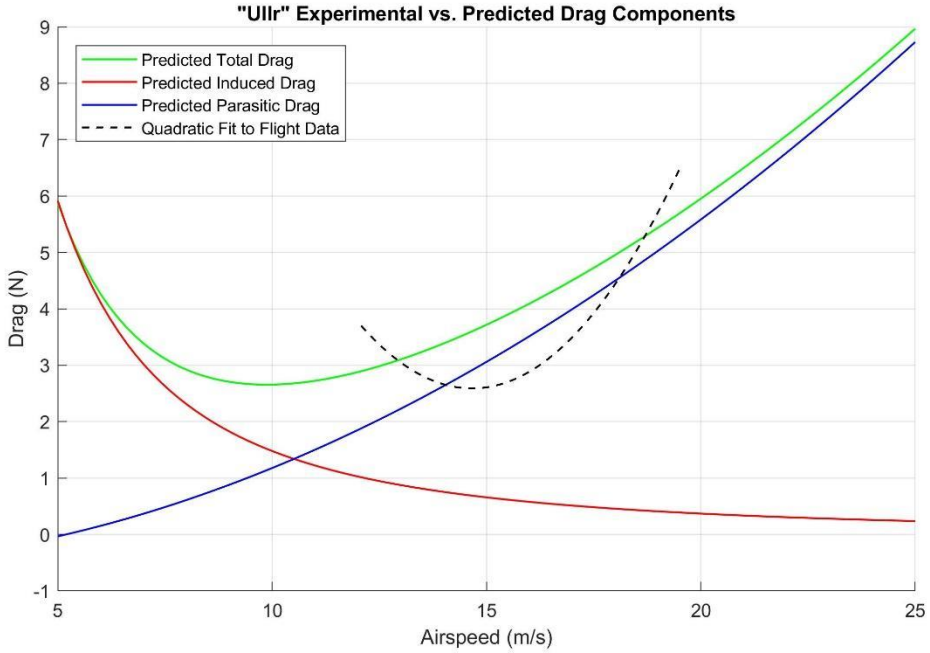

Figure 5.3.9: Experimental vs. predicted drag for "Ullr"

The plots for "Strato Surfer" and "Thor" show the successful implementation of the component drag build up method to predict drag. In section 5.1, the data for "Ullr" was deemed unreliable, and additional glide tests need to be performed. The divergence of the predicted drag from the measured drag at the extreme velocities in the case of the "Strato Surfer" and "Thor" can be rectified by collecting more data at the top and bottom of the velocity envelopes. The presence of more data points would improve the quadratic fit described in section 5.1. It can therefore be concluded that it is possible to accurately determine drag of a small electric UAV using the component drag build up method. It is also concluded that glide tests are an effective method of measuring drag.

6. Conclusion

By accounting for the unique operating conditions of small electric UAVs, the component drag build up method can be implemented to determine drag. Drag values can be effectively measured using glide tests, and used to validate drag predictions. Glide tests were performed for three aircraft belonging to the University of Minnesota UAV lab to measure drag. The data was then used to adjust and validate the component drag build up method and confirm the efficacy of this method.

7. Acknowledgments

This research was financed by the University of Minnesota's undergraduate research opportunities program (UROP).

I am grateful to my mentor Dr. Demoz Gebre-Egziabher for giving me the opportunity to conduct this research and providing invaluable advice.

I am very thankful to Chris Regan from the University of Minnesota Unmanned Aerial Vehicle lab for his crucial support and advice throughout the research process.

I also wish to thank Curtis Olson from the University of Minnesota Unmanned Aerial Vehicle lab, who piloted the aircraft during the glide tests.

I am thankful to Kale Hedstrom for assisting me with the Akerman Hall wind tunnel.

I thank Dr. Ellen K. Longmire for her advice on boundary layer theory.

I am grateful to Jakow Wilhelm Heide for his assistance with test interval selection.

I also thank Sarah Weyrauch whose comments and suggestions improved this manuscript.

Finally, I am thankful to my parents Julia Heide and Dr. Carsten Heide for their ceaseless support and encouragement.

Appendix: Additional Figures

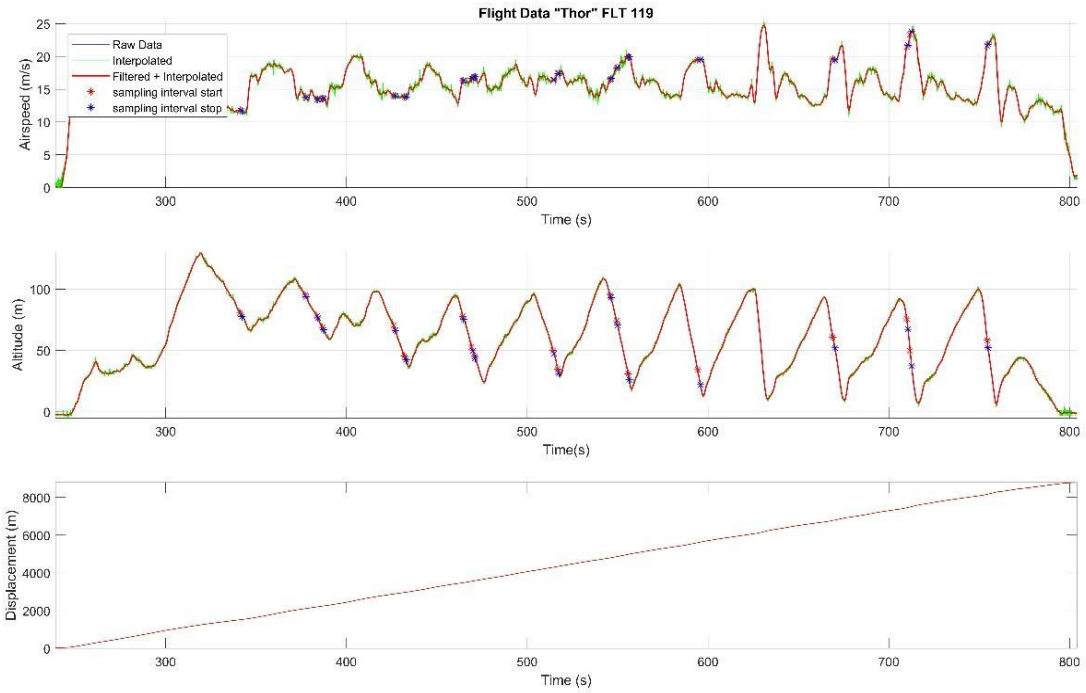

Figure A.1: Sample plot displaying a full flight.

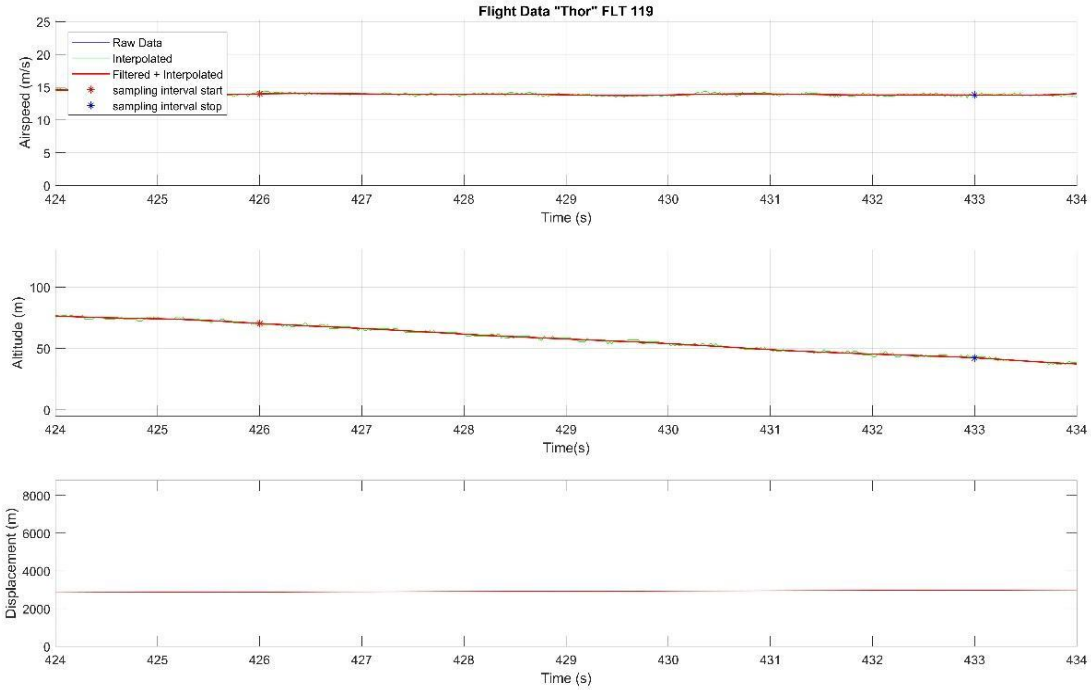

Figure A.2: Plot displaying a glide data range suitable for drag analysis.

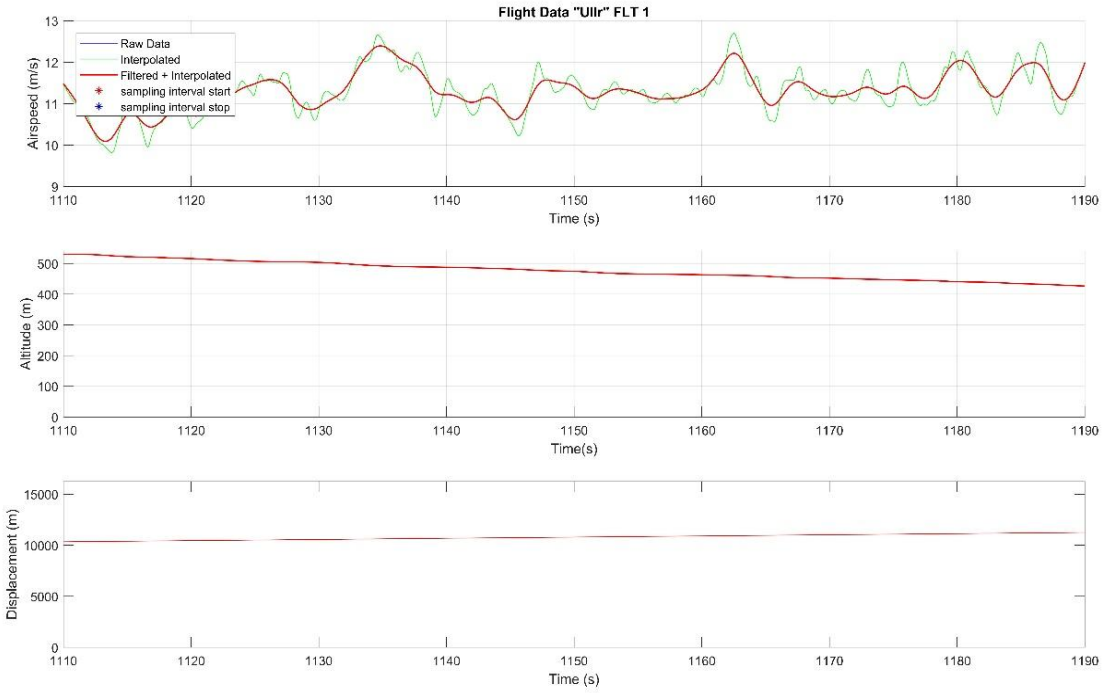

Figure A.3: Sample plot displaying a glide test range not suitable for drag analysis.

Bibliography

[1] Abbott, Ira H., and Albert E. Von Doenhoff. *Theory of Wing Sections: Including a Summary of Airfoil Data*. Dover Publications , (1959).

[2] Anderson, J. D., *Introduction to Flight* (3rd ed.). Boston, Massachusetts: McGraw-Hill, Chap. 4, (1989).

[3] Covert, Eugene E. *Thrust and Drag: Its Prediction and Verification*. American Institute of Aeronautics and Astronautics, (1985).

[4] Dam, C.p. Van. *Recent Experience with Different Methods of Drag Prediction*. Progress in Aerospace Science, vol. 35, no.8, pp. 751-798, (1999).

[5] Feagin, R. C. *Delta Method, an Empirical Drag Buildup Technique*. NASA, (1978).

[6] Heide, L., *Evaluating the Impact of Parasitic Drag on the Accuracy of Endurance Predictions*. University of Minnesota Digital Conservancy, University of Minnesota Twin Cities, http://hdl.handle.net/11299/199857, (2018)

[7] Hepperle, M., *Electric Flight-Potential and Limitations.* NATO (2012).

[8] Hoerner, Sighard F. *Fluid-Dynamic Drag: Theoretical, Experimental and Statistical Information*. Hoerner Fluid Dynamics, (1965).

[9] Kimberlin, Ralph D. *Flight Testing of Fixed-Wing Aircraft*. American Institute of Aeronautics and Astronautics, (2003).

[10] Kody, Frank, and Goetz Bramsfeld. *Small UAV Design Using an Integrated Design Tool*. Pennsylvania State University, International Journal of Micro Air Vehicles, (2012), pp. 151–163.

[11] McChlamroch, N. H., *Steady Aircraft Flight and Performance*. Princeton, New Jersey: Princeton University Press, (2011), pp. 35-47.

[12] Ostler, Jon N. et al., *Performance Flight Testing of Small, Electric Powered Unmanned Aerial Vehicles*. International Journal of Micro Air Vehicles, vol. 1, no. 3, (2009).

[13] "Parasite Drag Tool". OpenVSP, NASA, openvsp.org/wiki/doku.php?id=parasitedrag.

[14] Raymer, Daniel P. *Aircraft Design: A Conceptual Approach*. (2nd ed.). Washington, DC: AIAA, (1992) pp. 280-290.

[15] Roskam, Jan. *Airplane Design.* 2nd ed., DAR Corporation, (2003).

[16] Schlichting, Hermann. *Boundary-Layer Theory*. (7th ed.). Boston, Massachusetts: McGraw-Hill, (1979), pp. 640-642.

[17] Shaffer, D, and Turner, M. *Aerodynamic Prediction for Low Reynolds Numbers*. Department of Aerospace and Mechanical Engineering, University of Notre Dame, (2010).

[18] White, F. M. *Fluid Mechanics, 5th Edition.* New York: McGraw-Hill (2003).